JOURNAL OF MATERIALS SCIENCE 11 (1976) 2181–2188

The determination of Poisson's ratio compliances for polyethylene terephthalate sheets using a Michelson interferometer

I. WILSON*, A. CUNNINGHAM†, I. M. WARD
Department of Physics, University of Leeds, Leeds, UK

Two of the Poisson's ratio compliances have been determined for oriented polyethylene terephthalate (PET) sheet. The method adopted was to determine the fringe shift under load when the specimens were placed in one arm of a Michelson interferometer operating in a vertical fringe mode. Data obtained for the specimens in air and in a water bath, with two polarization directions, can be used to provide two independent measurements of each compliance. Good agreement was shown between these measurements, and the values for the compliance constants are reasonable on physical grounds, as well as being consistent with previous work on PET fibres.

1. Introduction

The determination of the Poisson's ratios of oriented polymers is often a vital link in the information required to formulate any understanding of their mechanical behaviour in terms of their structure. Poisson's ratios can also play an important part in the deformation which occurs in technological situations, for example, where polymers are being used in conjunction with other materials in some engineering application.

In spite of these considerations, there are comparatively few investigations in this area. Some of the most extensive work has been carried out by Saunders and co-workers on uniaxially oriented low-density polyethylene sheets [1–3]. The technique was based on a lateral contraction extensometer, in which rigid feelers rested lightly against the specimen sides. A contemporaneous investigation, also on uniaxially oriented low-density polyethylene, was that of Ladizesky and Ward [4], who measured photographically the deformation of a fine pattern of grid lines deposited on the sheet surface by vacuum deposition of aluminium.

There are a number of earlier determinations of the Poisson's ratios for polymer fibres and monofilaments. These involve the techniques of optical diffraction and mercury displacement adopted by Davis [5] and Frank and Ruoff [6], respectively, for nylon fibres. More extensive studies on nylon, polyethylene, polyethylene terephthalate and polypropylene were also made by the transverse compression of monofilaments [7–9].

In the present paper, we describe the determination of two of the three Poisson's ratio compliance constants for one-way drawn polyethylene terephthalate sheets. As the sheet is transparent, with a high degree of optical clarity and a conveniently small thickness, it was considered appropriate to use an optical interference technique where high accuracy (~ wavelength of light) can be obtained.

The results are of interest in that they complement previous measurements of extensional and shear compliances of similar sheets [10] and also relate to the earlier studies of mechanical anisotropy of polyethylene terephthalate fibres and monofilaments.

2. Theory

2.1. Elastic constants

The mechanical properties of an anisotropic elastic solid for small strains can be defined by the gen-

*Present address: Toll Bar Comprehensive School, Grimsby, UK.
†Present address: I.C.I. Corporate Laboratory, Runcorn, UK.

eralized Hooke's law relating strains ϵ_p to stresses σ_q:

$$\epsilon_p = S_{pq}\sigma_q, \quad \sigma_q = C_{qp}\epsilon_p \tag{1}$$

where S_{pq}, C_{qp} are the compliance and stiffness constants respectively, and p, q, take values 1, 2, ... 6. In the present study and polymer is subjected to constant load, and the corresponding strains are measured. It is therefore convenient to work in terms of the compliance constants S_{pq}.

The one-way drawn polyethylene terephthalate sheets possess orthorhombic symmetry. This has been discussed in detail elsewhere [10, 11]. There are, therefore, nine independent compliance constants. We choose a set of Cartesian axes 1, 2, 3; such that the 3 direction is parallel to the initial draw direction and the 1 direction is in the plane of the sheet perpendicular to the initial draw direction. The compliance matrix is then

$$S_{pq} = \begin{pmatrix} S_{11} & S_{12} & S_{13} & 0 & 0 & 0 \\ S_{12} & S_{22} & S_{23} & 0 & 0 & 0 \\ S_{13} & S_{23} & S_{33} & 0 & 0 & 0 \\ 0 & 0 & 0 & S_{44} & 0 & 0 \\ 0 & 0 & 0 & 0 & S_{55} & 0 \\ 0 & 0 & 0 & 0 & 0 & S_{66} \end{pmatrix} \tag{2}$$

and the Poisson's ratio compliance constants are S_{12}, S_{13} and S_{23}. In this paper we are concerned with the measurement of S_{12} and S_{23} only.

2.2. The photoelastic experiment

Consider that a sample of thickness t is inserted into one arm of an interferometer, which has air only in both paths, to produce m fringe shifts where

$$m\lambda = (n_i - 1)2t \tag{3}$$

n_i is the refractive index of the sample in the direction of the electric vector of the polarized monochromatic light at the wavelength λ. When the sample extends under load, the resultant fringe shift Δm is given by

$$\Delta m = \frac{2}{\lambda}[(n_i - 1)\Delta t + t\Delta n_i] \tag{4}$$

where Δt, Δn_i are the changes in thickness and refractive index respectively.

For an applied stress σ applied along the initial draw direction 3, the resultant change in thickness Δt_3

$$\Delta t_3 = S_{23} t \sigma_3. \tag{5a}$$

Similarly for a stress σ applied along the 1 direction we have

$$\Delta t_1 = S_{21} t \sigma_1. \tag{5b}$$

The situation regarding the changes in refractive index requires rather more attention. Following Nye [12], the ellipsoid which defines the refractive indices (the indicatrix) has the equation

$$\frac{x_1^2}{n_1^2} + \frac{x_2^2}{n_2^2} + \frac{x_3^2}{n_3^2} = 1 \tag{6}$$

where x_1, x_2, x_3, the principal axes of the dielectric constant tensor, are chosen to coincide with the 1, 2, 3 axes defined in Section 2.1 above, and n_1, n_2, n_3 are the principal refractive indices. The equation of this ellipsoid may also be written as

$$B_{ij}x_i x_j = 1 \tag{7}$$

where B_{ij} is the relative dielectric impermeability tensor.

Then the small changes in refractive index produced by stress can be conveniently represented as small changes in the coefficients B_{ij} and we have

$$\Delta B_{ij} = \pi_{ijkl}\sigma_{kl} \tag{8}$$

where σ_{kl} are the components of stress and π_{ijkl} is a fourth rank tensor describing the photoelastic behaviour. In this paper we are concerned only with normal stresses applied along principal axes. We can, therefore, adopt a contracted nomenclature with the normal stresses σ_{ij} represented by σ_i (as in Equation 1 above) and the changes in the coefficients along the principal axes ΔB_{ij} given by

$$\Delta B_{ij} = \Delta B_i = \pi_{ij}\sigma_j. \tag{9}$$

Again, since

$$B_i = \frac{1}{n_i^2}, \quad \Delta B_i = \frac{-2}{n_i^3}\Delta n_i$$

and we can write

$$\Delta n_i = \pi'_{ij}\sigma_j \tag{10}$$

where we have taken up the factor $-2/n_i^3$ in the definition of our simplified photoelastic constant matrix π'_{ij}.

Combining Equations 1 and 10 with Equation 4 we can then express the fringe shift in the air

interferometer formally as

$$\Delta m_a^{ij} = \frac{2t}{\lambda}[(n_i - 1)S_{2j} + \pi'_{ij}]\sigma_j. \quad (11)$$

We have adopted a superscript notation for Δm which corresponds exactly to the subscript notation for the π'_{ij}. It is also to be noted that we are only concerned in these measurements with the compliance constants S_{2j}, where $j = 1, 3$. Similarly for an interferometer with a water cell in which the sample can be immersed in one beam the fringe shift is given by

$$\Delta m_w^{ij} = \frac{2t}{\lambda}[(n_i - 1.33)S_{2j} + \pi'_{ij}]\sigma_j. \quad (12)$$

There are, therefore, eight different experiments which can be performed very simply. First, we can choose polarization conditions with the electric vector along either the 3 or 1 direction for the sample loaded along the 3 or 1 directions. Secondly the experiments can be undertaken with the sample in air or immersed in water. For the former situation these experiments yield the following fringe shifts which are denoted by the suffix a.

(i) *Sample loaded along 3 direction*

(a) Electric vector along 3 direction

$$\Delta m_a^{33} = \frac{2t}{\lambda}[(n_3 - 1)S_{23} + \pi'_{33}]\sigma_3 \quad (13)$$

(b) Electric vector along 1 direction

$$\Delta m_a^{13} = \frac{2t}{\lambda}[(n_1 - 1)S_{23} + \pi'_{13}]\sigma \quad (14)$$

(ii) *Sample loaded along 1 direction*

(a) Electric vector along 3 direction

$$\Delta m_a^{31} = \frac{2t}{\lambda}[(n_3 - 1)S_{21} + \pi'_{31}]\sigma_1 \quad (15)$$

(b) Electric vector along 1 direction

$$\Delta m_a^{11} = \frac{2t}{\lambda}[(n_1 - 1)S_{21} + \pi'_{11}]\sigma_1 \quad (16)$$

For the case where the sample is immersed in water the corresponding fringe shifts are denoted by the suffix w and are given by the equations

$$\Delta m_w^{33} = \frac{2t}{\lambda}[(n_3 - 1.33)S_{23} + \pi'_{33}]\sigma_3 \quad (17)$$

$$\Delta m_w^{13} = \frac{2t}{\lambda}[(n_1 - 1.33)S_{23} + \pi'_{13}]\sigma_3 \quad (18)$$

$$\Delta m_w^{31} = \frac{2t}{\lambda}[(n_3 - 1.33)S_{21} + \pi'_{31}]\sigma_1 \quad (19)$$

and

$$\Delta m_w^{11} = \frac{2t}{\lambda}[(n_1 - 1.33)S_{21} + \pi'_{11}]\sigma_1. \quad (20)$$

It is, therefore, possible to make two independent determinations of each of the compliance constants. Two values for S_{23} are obtained from experiments which correspond to Equations 13 and 17, and 14 and 18, respectively. Two values for S_{21} come from the experiments corresponding to Equations 15 and 19, and 16 and 20, respectively.

We have,

$$S_{23} = \frac{\lambda(\Delta m_a^{33} - \Delta m_w^{33})}{0.66t\sigma_3} = \frac{\lambda(\Delta m_a^{13} - \Delta m_w^{13})}{0.66t\sigma_3} \quad (21)$$

and

$$S_{21} = \frac{\lambda(\Delta m_a^{31} - \Delta m_w^{31})}{0.66t\sigma_1} = \frac{\lambda(\Delta m_a^{11} - \Delta m_w^{11})}{0.66t\sigma_1} \quad (22)$$

These experiments also yield values for the photoelastic constants π'_{11}, π'_{33}, π'_{13} and π'_{31}, which are given by the following equations

$$\pi'_{11} = \frac{\lambda}{2t\sigma_1}\left[\Delta m_a^{11} - \frac{(n_1 - 1)(\Delta m_a^{11} - \Delta m_w^{11})}{0.33}\right] \quad (23)$$

$$\pi'_{33} = \frac{\lambda}{2t\sigma_3}\left[\Delta m_a^{33} - \frac{(n_3 - 1)(\Delta m_a^{33} - \Delta m_w^{33})}{0.33}\right] \quad (24)$$

$$\pi'_{13} = \frac{\lambda}{2t\sigma_3}\left[\Delta m_a^{13} - \frac{(n_1 - 1)(\Delta m_a^{13} - \Delta m_w^{13})}{0.33}\right] \quad (25)$$

$$\pi'_{31} = \frac{\lambda}{2t\sigma_1}\left[\Delta m_a^{31} - \frac{(n_3 - 1)(\Delta m_a^{31} - \Delta m_w^{31})}{0.33}\right] \quad (26)$$

3. Experimental

3.1. Sample preparation

Samples in the form of 10 cm long strips were prepared with microtomed edges. This was important when cutting specimens with their lengths at right angles to the initial draw direction in the sheet, where a very rough initial edge was produced.

The length to width ratio was of the order of 25:1 to eliminate any constraints imposed by the

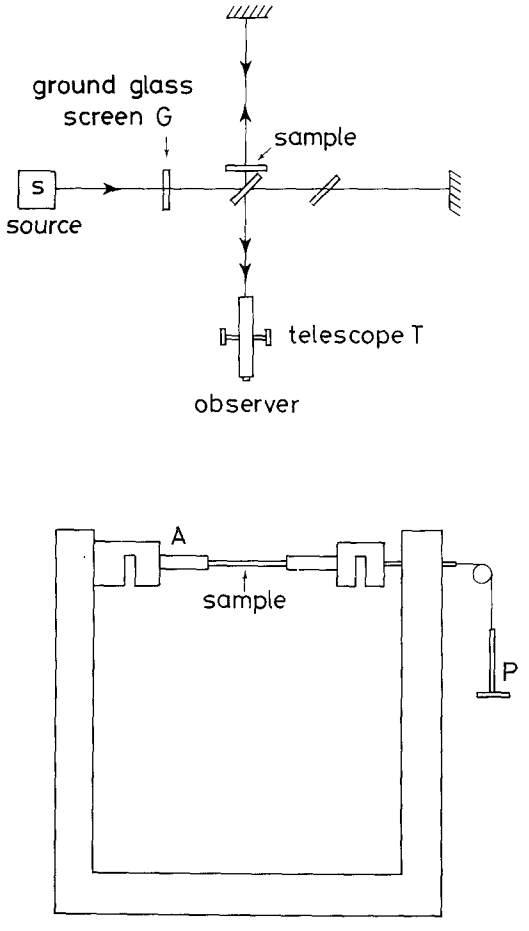

Figure 1 Interferometric arrangement and apparatus for measuring Poisson's ratio.

grips. The cross-sectional areas were determined by measuring the width and thickness of the samples with a travelling microscope and a micrometer respectively. Samples with cross-sectional areas in the range 6×10^{-3} to 2×10^{-3} cm^2 were measured.

3.2. Apparatus

The basic interferometer arrangement is shown in Fig. 1. The load is applied directly to the sample by placing weights on the pan P. The interferometer is illuminated by a sodium lamp, S, the ground glass screen, G providing a diffuse source. The fringes were viewed with a telescope T, in front of which was placed a polarizer. The apparatus was maintained level using two spirit levels.

The sample is held between two clamps, each supported by a vertical column so that the two columns form a yoke arrangement. The interferometer is positioned within this yoke, such that the sample is in one of the arms of the interferometer. A wire, attached to the moveable clamp, passes over a pulley and the load is applied directly to the sample by placing weights on the pan fixed to the end of the wire. The slots in the clamps enable the sample to be immersed in a trough of water.

The interferometer was adjusted to operate in a vertical fringe mode as opposed to the more usual concentric ring mode. This requires that the two mirrors are slightly offset from being at right angles to each other. This produces the situation of interference by a thin wedge and hence vertical linear fringes are produced.

The moveable clamp is free to rotate about its major axis, allowing the sample to be twisted slightly about its vertical position. As this is done, the fringe shift goes through a minimum condition corresponding to the minimum path length increase produced by the presence of the sample. In this way it is possible to ensure that the sample is aligned in the vertical plane.

3.3. Measurements

Fringe shifts were determined for a series of loads up to contractions of about 0.3% and 1% for loads applied along the draw direction (0° direction) and perpendicular to this (the 90° direction) respectively. Having determined the fringe shift for a given applied load, the load was removed and the displaced fringes observed to return to their zero load position. The vertical alignment of the sample under extension was always checked as there was a tendency to twist which can produce a false fringe shift.

Measurements were made for both vertical and horizontal polarization in both air and water. To check the effect of the sample being immersed in water, measurements were made of sample extension as a function of load. This was done by measuring the displacement of the moveable clamp with an extensometer. For a range of loads it was verified that the sample extension was unaffected by the surrounding water. This is in accord with expectations, since it is known from previous work that the mechanical properties of PET are only affected by moisture at elevated temperatures, when the material approached the glass transition.

The time dependence of the mechanical response is very small in PET at room temperature. In a previous paper [10] it was shown to be $\sim 3\%$ in S_{11} and S_{33} from 10 s to 10^3 secs. Although this is not likely to be detectable within the accu-

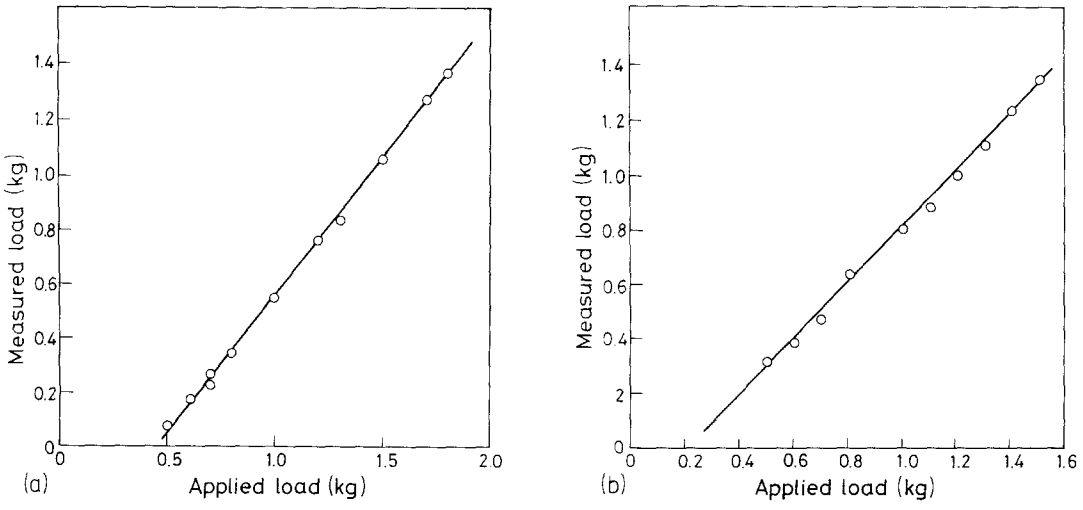

Figure 2 Calibration of load applied to sample: (a) for loads applied paralled to draw direction; (b) for loads applied at 90° to draw direction.

racy of the present measurements, the fringe shifts were always determined as near as possible to 10 secs after the application of the load.

4. Results

Preliminary measurements established that there was a very satisfactory linear relationship between the fringe shift and the applied load. The straight lines did not, however, pass through the zero load point. For both sample directions it was therefore decided to carry out a direct calibration of the relationship between the stress applied to the sample and the applied load. This was done be inserting a piezoelectric transducer into the point A, and comparing the load acting on the specimen directly with the applied load. The results of this calibration are shown in Fig. 2a and b. It can be seen that although the initial frictional constraints differ for the two sample directions, the relationship between the applied load and that measured by the transducer is a linear one with a proportionality constant which is unity within the experimental error.

This calibration was used to produce the final plots of fringe shift as a function of the load applied to the sample. Results for the case where the load was applied at 90° to the draw direction are shown for two samples in Figs. 3 and 4. Similarly, the results for two samples with the load applied in the draw direction are shown in Figs. 5 and 6. It can be seen that in nearly all cases the results can be very well represented by a straight line passing through the origin. The data are most definitive where the fringe shifts are large for comparatively small applied loads, e.g. Figs. 3 and 4 for the cases $\Delta m_a{}^{31}$ and $\Delta m_w{}^{31}$. Where the fringe shifts are very much smaller, the results are clearly less reliable, and there is one case $\Delta m_w{}^{33}$, shown in Fig. 5 and 6, where it does not appear

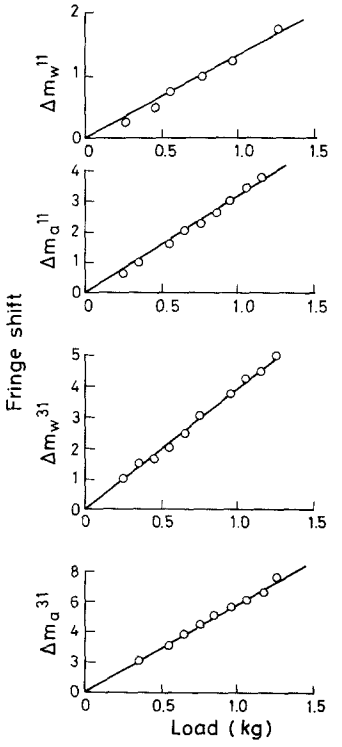

Figure 3 Fringe shift as a function of applied load (sample A, load at 90° to draw direction).

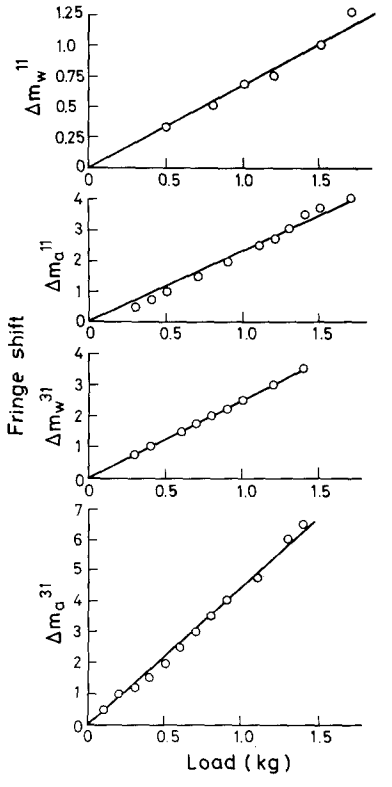

Figure 4 Fringe shift as a function of applied load (sample B, load at 90° to draw direction).

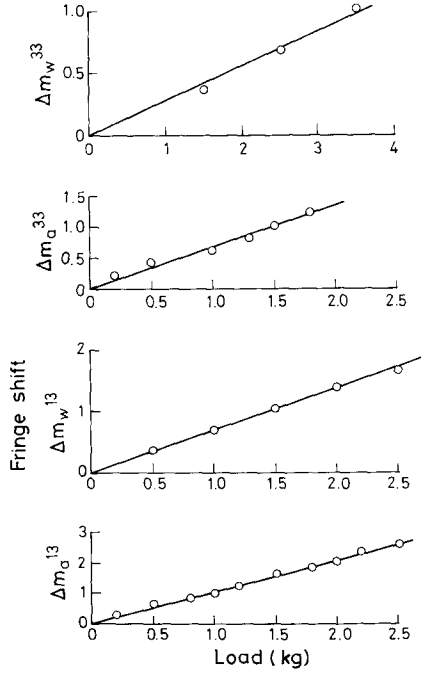

Figure 5 Fringe shift as a function of applied load (sample A, load parallel to draw direction).

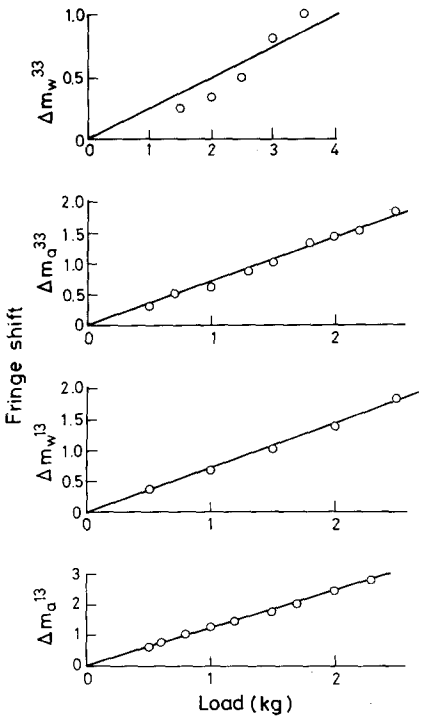

Figure 6 Fringe shift as a function of applied load (sample B, load parallel to draw direction).

satisfactory to include the results in the final determination of the compliance constants.

The results obtained from the gradients in Figs. 3 to 6 are summarized in Tables I and II. Using Equations 21 and 22 we can make two determinations of S_{21} and S_{23} for each sample. These are shown in Table III, with the values of S_{33} obtained from $\Delta m_w{}^{33}$ shown in brackets. As already mentioned these results are unreliable although they, in fact, do appear to just show a greater scatter about the same mean value. The final average values for the compliances S_{21} and S_{23} are S_{21} =

TABLE I Fringe shift data for load applied at 90° to draw direction

Sample	Mode	Δm_a^{31}	Δm_w^{31}	Δm_a^{11}	Δm_w^{11}
A	Fringe shift per kg	4.40	2.50	2.30	0.65
A	Fringe shift per unit stress 10^{-7} m^2 N^{-1}	2.76	1.57	1.45	0.41
B	Fringe shift per kg	5.9	3.9	3.25	1.3
B	Fringe shift per unit stress 10^{-7} m^2 N^{-1}	2.8	1.86	1.60	0.62

TABLE II Fringe shift data for load applied parallel to draw direction

Sample	Mode	Δm_a^{13}	Δm_w^{13}	Δm_a^{33}	Δm_w^{33}
A	Fringe shift per kg	1.05	0.70	0.68	0.28
A	Fringe shift per unit stress 10^{-8} m^2 N^{-1}	3.16	2.10	2.05	0.84
B	Fringe shift per kg	1.20	0.70	0.70	0.25
B	Fringe shift per unit stress 10^{-8} m^2 N^{-1}	2.90	1.69	1.69	0.60

$-3.8 \pm 0.4 \times 10^{-10}$ m^2 N^{-1} and $S_{23} = -0.37 \pm 0.02 \times 10^{-10}$ m^2 N^{-1}.

Although in principle the experiments should also yield values for the photoelastic constants, inspection of the actual results in terms of Equations 23 to 26 shows that these depend on comparatively small differences between large quantities, and with the exception of π'_{13} show a large scatter. These calculations were therefore not proceeded with.

5. Discussion

The values obtained for S_{21} and S_{23} are of most interest when compared with the other compliance constants for the orthorhombic sheet, and with similar compliance constants for fibres. Table IV shows some collected values of compliance constants and Poisson's ratios. The values for S_{11} and S_{33} were obtained from measurements of extensional creep in a dead loading creep machine, and refer to the 10 sec response at 0.1% strain. The value of S_{13} was obtained from the deformation of an electron microscope grid printed on the surface of the sample, and its determination is described in a separate publication [13]. The values of the fibre compliance constants are taken from a previous publication [8]. Because of the different techniques employed to determine different constants the values for the different elastic constants are not exactly comparable. Care was taken to measure the 10 sec response in all cases, but there are some differences with regard to stain level and possible non-linearity. The present data show no signs of non-linearity, although such efffects were seen in the determinations of S_{11}, S_{33} and S_{13}. It must be emphasized, however, that the effects are very small ($\sim 5\%$) at the low levels of strain involved, compared with the differences between the different compliance constants. Table IV shows that these differ in some cases by more than one order of magnitude. With minor reservations, we can therefore proceed to discuss the general nature of the mechanical anisotropy.

In the first instance it can be commented that the magnitudes of S_{21} and S_{23} are certainly in keeping with expectations on physical grounds, based on the values of the other elastic constants S_{11}, S_{33} and S_{13}. The orthorhombic sheet is very anisotropic, with S_{33}, the compliance along the draw direction, being about seven times smaller than S_{11}, that perpendicular to the draw direction. This is to be expected because S_{33} will involve some element of bond stretching and bond bending, whereas S_{11} can be attributed largely to transverse dispersion forces. Thus it is not unreasonable that the stiffness along the draw direction is about an order of magnitude greater than that perpendicular to the draw direction. It also follows from such considerations that if the polymer is stressed

TABLE III Values of S_{21} and S_{23} (10^{-10} m^2 N^{-1})

Sample	S_{21}	Average value of S_{21}	S_{23}	Average value of S_{23}
A	$-4.2, -3.7$		$-0.35, (-0.40)$	
		-3.8 ± 0.4		-0.37 ± 0.02
B	$-3.7, -3.6$		$-0.38, (-0.34)$	

TABLE IV Collected values of compliance constants ($\times 10^{-10}$ m^2 N^{-1}), and Poisson's ratios

	S_{21}	S_{23}	S_{13}	S_{11}	S_{33}	$\nu_{21} = \frac{-S_{21}}{S_{11}}$	$\nu_{31} = \frac{-S_{13}}{S_{11}}$	$\nu_{23} = \frac{-S_{23}}{S_{33}}$	$\nu_{13} = \frac{-S_{13}}{S_{33}}$
Sheet	-3.8	-0.37	-0.18	4.0	0.76	0.95	0.05	0.48	0.26
Fibre A	-3.9	–	-0.47	8.9	1.1	0.44	0.05	–	0.43
Fibre B	-5.8	–	-0.31	16.1	0.71	0.36	0.02	–	0.44

in a direction perpendicular to the draw direction, that the major contraction is likely to take place in the direction perpendicular to the chain orientation (the 2 direction) rather than parallel to the draw direction (the 3 direction). Thus we would expect the magnitude of S_{21} to be much greater than that of S_{23}. The value of S_{13} is similar to that of S_{23} which is consistent with this line of argument, i.e. the comparative difficulty of deformation in the 3 direction, compared with the 1 and 2 directions. The Poisson's ratios reflect the same argument, and in particular ν_{31} has the very small value of 0.05.

Secondly, the values of S_{21} and S_{23} for the orthorhombic sheet are in line with the values of the corresponding compliance constants for fibres. This can be seen by direct comparison of values for S_{21} (-3.8 for sheet compared with -3.9 and -5.8 for fibres) and by the comparability of S_{23} and S_{13} for sheet (-0.37 and -0.18) with fibre values of -0.47 and -0.31 for S_{13}. The comparison of the Poisson's ratios for the sheet and fibres brings out their comparability more clearly and follows from the order of magnitude arguments developed in the last paragraph. A more detailed comparison between sheet and fibres required knowledge of all the elastic constants.

6. Conclusions

A novel method has been tested which determines two Poisson's ratio compliances for transparent polymer sheet of orthorhombic symmetry. The results for polyethylene terephthalate sheets show reasonable consistency, and the actual values obtained are in good accord with expectations on physical grounds.

References

1. M. W. DARLINGTON and D.W. SAUNDERS, *J. Phys. E.* **3** (1970) 511.
2. *Idem, J. Phys. D.* **3** (1970) 535.
3. D. CLAYTON, M. W. DARLINGTON and M. M. HALL, *J. Phys. E.* **6** (1973) 218.
4. N. H. LADIZESKY and I. M. WARD, *J. Macromol. Sci. Phys.* **B5** (1971) 661.
5. V. DAVIS, *J. Text. Inst.* **50** (1960) 1688.
6. F. I. FRANK and A. L. RUOFF, *Text. Res. J.* **28** (1958) 213.
7. D. W. HADLEY, I. M. WARD and J. WARD, *Proc. Roy. Soc.* **A285,** (1965) 275.
8. P. R. PINNOCK, I. M. WARD and J. M. WOLFE, *ibid.* **A291** (1966) 267.
9. D. W. HADLEY, P. R. PINNOCK and I. M. WARD, *J. Mater. Sci.* **4** (1969) 152.
10. N. H. LADIZESKY and I. M. WARD, *ibid.* 8 (1973) 980.
11. M. KASHIWAGI, A. CUNNINGHAM, A. J. MANUEL and I. M. WARD, *Polymer 14,* (1973) 111.
12. J. F. NYE, "Physical Properties of Crystals" (Clarendon Press, Oxford, 1957).
13. I. WILSON, N. H. LADIZESKY and I. M. WARD *J. Mater. Sci.* **11** (1976) 2177.

Received 13 April and accepted 4 May 1976.